Skillful regional prediction of Arctic sea ice on seasonal timescales

Mitchell Bushuk[1], Rym Msadek[2], Michael Winton[3], Gabriel A. Vecchi[1,4], Rich Gudgel[3], Anthony Rosati[3], and Xiaosong Yang[3]

[1]Atmospheric and Oceanic Sciences Program, Princeton University, Princeton, New Jersey, USA

[2]CNRS/CERFACS, CECI UMR 5318, Toulouse, France

[3]National Oceanic and Atmospheric Administration/Geophysical Fluid Dynamics Laboratory, Princeton University, Princeton, New Jersey, USA

[4]Department of Geosciences, Princeton University, Princeton, New Jersey, USA

Key points:

- Coupled dynamical prediction system skillfully predicts regional sea-ice extent on seasonal timescales
- Ocean subsurface temperature initialization yields North Atlantic regional winter skill at lead times of 5–11 months
- Sea-ice thickness initialization provides a key source of summer regional skill at lead times of 1–4 months

Corresponding author: Mitch Bushuk, Atmospheric and Oceanic Sciences Program, Princeton University, 201 Forrestal Road, Princeton, New Jersey, USA, 08540. E-mail: mbushuk@princeton.edu

Recent Arctic sea ice seasonal prediction efforts and forecast skill assessments have primarily focused on pan-Arctic sea-ice extent (SIE). In this work, we move towards stakeholder-relevant spatial scales, investigating the regional forecast skill of Arctic sea ice in a Geophysical Fluid Dynamics Laboratory (GFDL) seasonal prediction system. Using a suite of retrospective initialized forecasts spanning 1981–2015 made with a coupled atmosphere-ocean-sea ice-land model, we show that predictions of detrended regional SIE are skillful at lead times up to 11 months. Regional prediction skill is highly region and target month dependent, and generically exceeds the skill of an anomaly persistence forecast. We show for the first time that initializing the ocean subsurface in a seasonal prediction system can yield significant regional skill for winter SIE. Similarly, as suggested by previous work, we find that sea-ice thickness initial conditions provide a crucial source of skill for regional summer SIE.

1. Introduction

Arctic sea ice has undergone rapid changes over the satellite era, characterized by a decline in pan-Arctic September sea-ice extent (SIE) of roughly -14% per decade [*Serreze et al.*, 2007; *Cavalieri and Parkinson*, 2012; *Stroeve et al.*, 2014a], substantial thinning [*Rothrock et al.*, 1999; *Kwok and Rothrock*, 2009], a transition from multi-year to first-year ice [*Rigor and Wallace*, 2004; *Maslanik et al.*, 2011], and longer melt seasons [*Perovich and Polashenski*, 2012; *Stroeve et al.*, 2014a]. These striking changes and their implications for stakeholders have sparked research interest in the seasonal prediction and predictability of Arctic sea ice. Seasonal prediction skill for detrended pan-Arctic SIE has been assessed in a number of global climate model (GCM)-based forecast systems. These studies, based on suites of initialized retrospective forecasts (hindcasts), report significant forecast skill relative to the linear trend at lead times of 1–6 months, depending on the target month and model used [*Wang et al.*, 2013; *Chevallier et al.*, 2013; *Sigmond et al.*, 2013; *Merryfield et al.*, 2013; *Msadek et al.*, 2014; *Peterson et al.*, 2015; *Blanchard-Wrigglesworth et al.*, 2015; *Guemas et al.*, 2016]. Statistical forecast methods have also been shown to skillfully predict detrended pan-Arctic SIE at leads times up to 6 months [*Lindsay et al.*, 2008; *Stroeve et al.*, 2014b; *Schröder et al.*, 2014; *Wang et al.*, 2016; *Yuan et al.*, 2016; *Petty et al.*, 2017].

In parallel with the development of these quasi-operational dynamical prediction systems, a number of "perfect model" studies, which examine how well a model can predict itself, have been performed to quantify upper bounds for the forecast skill achievable in such systems. These perfect model studies have shown that pan-Arctic SIE is poten-

tially predictable at 12–24 month lead times, substantially longer than the current skill of GCM-based prediction systems [*Koenigk and Mikolajewicz*, 2009; *Holland et al.*, 2011; *Blanchard-Wrigglesworth et al.*, 2011a; *Tietsche et al.*, 2014; *Germe et al.*, 2014]. Analogous to the so-called "quiet revolution" in numerical weather prediction [*Bauer et al.*, 2015], closing this prediction skill gap will require improvements in both model physics and initial conditions (ICs).

These studies have defined baselines for the current and potential seasonal forecast skill of pan-Arctic SIE. While this body of work represents a crucial first step, its utility is somewhat limited for stakeholders, who are primarily interested in sea-ice predictions on regional and sub-regional spatial scales. Regional sea-ice predictions are a pressing need for a broad stakeholder group, including Northern communities [*Ford and Smit*, 2004], wildlife [*Regehr et al.*, 2007], shipping industries [*Smith and Stephenson*, 2013; *Melia et al.*, 2016; *Pizzolato et al.*, 2016; *Laliberté et al.*, 2016], fisheries [*Wyllie-Echeverria and Wooster*, 1998], and natural resource industries [*Jung et al.*, 2016]. The decline of regional SIE is ubiquitous in the Arctic, with statistically significant negative SIE trends in all regions except for the Bering Sea, which has a small positive trend that is not statistically significant [*Cavalieri and Parkinson*, 2012].

Baselines for current and potential regional Arctic SIE prediction skill in dynamical forecast systems have yet to be thoroughly established. The study of *Sigmond et al.* [2016] demonstrated skillful predictions of detrended regional ice advance and retreat dates, with notably high skill for advance dates in Hudson Bay, Baffin Bay/Labrador Sea, and the Chukchi Sea. *Krikken et al.* [2016] investigated detrended regional sea-ice area

predictions (using three initialization months), and found skillful forecasts up to 6-month lead times for the Barents/Kara Seas and the Northeast passage region. The work of *Day et al.* [2014a] identified the seasonal-ice zones of the North Atlantic sector as the regions with highest potential SIE predictability (at lead times of 1.5–2.5 years). *Yeager et al.* [2015] additionally demonstrated skillful predictions of decadal SIE trends in this sector, which they attributed to predictable variations in the Atlantic thermohaline circulation.

In this work, we present the first comprehensive assessment of regional Arctic SIE prediction skill within a coupled dynamical prediction system. Using a suite of retrospective seasonal forecasts, we examine regional SIE skill in fourteen Arctic regions for all target months and lead times of 0–11 months. We study the physical mechanisms underlying this regional skill, identifying critical roles for initialization of subsurface ocean temperature and sea-ice thickness in regional predictions of winter and summer SIE, respectively. Finally, implications for future dynamical prediction systems are discussed.

2. Methods

2.1. The GFDL Prediction System

This study is based on a suite of retrospective seasonal forecasts spanning 1981–2015 made with one of the Geophysical Fluid Dynamics Laboratory (GFDL) prediction systems. The prediction system consists of a fully-coupled atmosphere-land-sea ice-ocean GCM with initial conditions (ICs) from a coupled data assimilation system. The forecast model is the GFDL Forecast-oriented Low Ocean Resolution [FLOR; *Vecchi et al.*, 2014] model, which employs a relatively-high horizontal resolution of 0.5° in the atmosphere and land components, and 1° resolution in the ocean and sea ice components. The sea ice

model of FLOR is the Sea Ice Simulator version 1 [SIS1; *Delworth et al.*, 2006]. This model uses an elastic-viscous-plastic rheology for the calculation of internal ice forces [*Hunke and Dukowicz*, 1997], an ice-thickness distribution with five thickness categories [*Bitz et al.*, 2001], and a three-layer thermodynamic formulation with one snow layer and two ice layers [*Winton*, 2000]. The FLOR prediction system exhibits seasonal forecast skill for a diverse set of climate applications, including tropical cyclone activity [*Vecchi et al.*, 2014], pan-Arctic SIE [*Msadek et al.*, 2014], surface-air temperature and precipitation over land [*Jia et al.*, 2015], and regional sea-surface temperature [SST; *Stock et al.*, 2015].

The seasonal forecasts are initialized using an Ensemble Kalman Filter coupled Data Assimilation system [ECDA; *Zhang et al.*, 2007]. The ECDA system assimilates subsurface ocean temperature and salinity data, satellite SST, and atmospheric reanalysis data from National Centers for Environmental Prediction. The subsurface ocean data comes from the World Ocean Database [*Levitus et al.*, 2013], the Global Temperature and Salinity Profile Programme [*Sun et al.*, 2010], and the Argo Program [*Roemmich et al.*, 2004]. These data sources comprise a wide variety of historical oceanic observations including expendable bathythermograph (XBT) data, conductivity-temperature-depth (CTD) data, moored buoy data (MRB), mechanical bathythermograph data (MBT), ocean station data (OSD; or so called "bottle" data), and autonomous ocean profiles (PFL; since the introduction of Argo floats in 2000). Note that ECDA does not directly assimilate any sea-ice concentration (SIC) or thickness (SIT) data. The ocean and sea ice ICs are taken directly from ECDA, whereas the atmosphere and land ICs are produced via a suite of "AMIP-style" atmosphere-land only simulations forced by observed SST and sea ice.

This technique is used to initialize the atmosphere and land components because FLOR employs a higher resolution in these components than ECDA, which was built on the CM2.1 model [*Delworth et al.*, 2006]. The ensemble forecast experiments are initialized with a twelve-member ensemble on the first of each month from January 1981 through December 2015 and run for one year. This suite of hindcasts allows us to assess the skill of this forecast system against nearly all of the available satellite SIC record, which begins in November 1978.

2.2. Forecast Skill Assessment

In this study, we assess the ability of the FLOR prediction system to predict regional SIE in the fourteen Arctic regions shown in Fig. 1. The regional domains are chosen following the *Day et al.* [2014a] definitions. We compute prediction skill scores for each region, target months from January–December, and lead times from 0–11 months. "Target month" refers to the month that we are trying to predict, and "lead time" refers to the number of months prior to the target month that the forecast was initialized. We verify our predictions against passive microwave satellite SIC observations from the National Snow and Ice Data Center (NSIDC). We use monthly-averaged SIC data processed using the NASA team algorithm [*Cavalieri et al.*, 1996], and regrid these data from the native NSIDC 25km polar stereographic grid onto the 1° GFDL sea-ice grid. The regridding was performed to avoid systematic SIE biases associated with the different land-sea masks of the two grids.

We assess prediction skill via the anomaly correlation coefficient (ACC). The ACC is the Pearson correlation coefficient between the predicted and observed regional SIE time

series. The predicted regional SIE is computed in two steps: (1) we compute the ensemble-mean predicted SIC; and (2) we compute an areal sum of all gridpoints in the region of interest with SIC $\geq 15\%$. In order to focus on skill relative to the long-term trend, we remove a linear trend forecast from the observed and predicted SIE time series before computing ACC values. The linear trend forecast is computed using only past data, and is updated each year. For the first three hindcast years (1982–1984), we assume a linear trend of zero. We test whether the ACC values are significantly greater than 0 using a t-test with a confidence level of 95%. The effective number of degrees of freedom for the t-test is given by $N^* = \frac{1-r_1 r_2}{1+r_1 r_2} N$, where $N = 34$ is the number of years in the timeseries, and r_1 and r_2 are the lag-1 year autocorrelation values for each time series [*Bretherton et al.*, 1999]. Using this approach, we compute significance thresholds for each region, target month, and lead time. These thresholds vary regionally between 0.29 and 0.38.

We compare our prediction skill to an anomaly persistence forecast, which is the forecast obtained by persisting the observed anomaly of the initial month up to the target month. The anomalies in the persistence forecast may be defined relative to either the long-term climatology or the long-term linear trend, depending on whether one is assessing skill for total anomalies or detrended anomalies, respectively. We also compared our prediction skill to a damped anomaly persistence forecast [*Van den Dool*, 2006]. In terms of ACC, anomaly persistence is slightly more skillful than damped anomaly persistence, which motivated its use as the baseline forecast in this study.

3. Results

3.1. Arctic Regional Prediction Skill

In Fig. 2, we plot the GFDL-FLOR Arctic regional prediction skill for detrended SIE. The prediction skill for total anomalies (non-detrended) is higher in all regions (see Fig. S1), due to predictability from negative regional SIE trends and the ability of the forecast system to capture these trends [*Msadek et al.*, 2014]. The detrended regional SIE forecast skill in Fig. 2 generically exceeds that of a persistence forecast (see triangles in Fig. 2). This indicates that there are dynamical sources of predictability beyond SIE anomaly persistence which this prediction system is able to capture. Interestingly, each Arctic region displays a unique correlation structure. These correlation structures are the result of three interrelated factors: (1) the inherent predictability of SIE in each region; (2) the accuracy of the forecast ICs; and (3) the ability of the model to dynamically evolve the IC fields and simulate regional SIE. Below, we highlight some key features of the regional SIE predictions.

Regional prediction skill is notably high for winter predictions of SIE in the North Atlantic sector. The Barents and Greenland-Iceland-Norwegian (GIN) Seas have statistically significant skill at lead times ranging from 5–9 months for target months of December–March (time series of January Barents SIE predictions are shown in Fig. S2). Labrador Sea skill is the highest of any region, with significant skill beyond 7 months for target months of December–July. These skillful long-lead regional winter predictions correspond to forecasts initialized the previous summer and spring, often in months with little sea-ice cover. Ahead in Section 3.2, we investigate the sources of skill for these winter SIE predictions. In contrast to the North Atlantic sector, the seasonal-ice zones of the North

Pacific Sector (the Bering Sea and Sea of Okhotsk) display little prediction skill beyond 3-month lead times.

The prediction system also displays significant summer SIE skill in the East Siberian, Laptev, Chukchi, and Beaufort Seas (time series of September East Siberian SIE predictions are shown in Fig. S2). The summer SIE predictions in these regions are skillful at lead times of 1–4 months, lacking the long-lead skill of the winter North Atlantic predictions. The East Siberian, Laptev, and Beaufort Seas each display a barrier of prediction skill, in which skill drops off sharply in a certain initialization month. For the East Siberian and Laptev seas, this skill barrier corresponds to forecasts initialized before May, whereas for the Beaufort Sea, the barrier corresponds to forecasts initialized before June. These skill barriers can be identified in the ACC plots as diagonal lines corresponding to initial months May and June, respectively. A similar predictability barrier has been identified in the work of *Day et al.* [2014a], which showed that perfect-model forecasts initialized in May lose skill more rapidly than forecasts initialized in July. The predictions also have skill for summer SIE in the Canadian Archipelago, however this result should be viewed cautiously given the coarse model grid and relatively small number of gridpoints in this region. We further investigate the sources of summer SIE prediction skill in Section 3.3, ahead.

In addition to skillfully predicting regional SIE minima and maxima, the forecasts also have skill in predicting melt season (June-July-August) and growth season (November-December) anomalies in Hudson Bay at lead times of 3–11 months. Forecast skill in

198 Baffin Bay, another region that rapidly transitions from being ice-covered to ice-free, is
199 substantially lower.

200 Pan-Arctic SIE represents the sum total of these diverse regional contributions. The
201 FLOR prediction system generally has skill in predicting detrended pan-Arctic SIE at
202 lead times of 1-5 months [*Msadek et al.*, 2014]. The month of June is a clear exception
203 to this, with low skill even for lead-0 predictions. The pan-Arctic correlation structure
204 displays two "lobes" of skill which peak in April and October, following the SIE maximum
205 and minimum, respectively (Fig. 2, upper left panel). Skill drops rapidly in the months
206 of June and December, which are the months when the ice edge transitions between the
207 Central Arctic and the seasonal-ice zones. The persistence forecast also displays a similar
208 two-lobe correlation structure (See Fig. S3), with low skill in June, July, November, and
209 December, indicating that the FLOR ACC structure is related to the inherent persistence
210 of pan-Arctic SIE anomalies. A similar link between persistence and predictability was
211 found in the perfect model study of *Day et al.* [2014a]. Note that FLOR's low June
212 prediction skill is not a generic feature of other dynamical prediction systems (compare
213 Fig. 5b of *Wang et al.* [2013], Figs. 1ab of *Merryfield et al.* [2013], Fig. 3b of *Sigmond*
214 *et al.* [2013] and Fig. 8a of *Peterson et al.* [2015]), however a similar decrease in skill
215 between September/October and November/December is seen in some systems [*Wang*
216 *et al.*, 2013; *Merryfield et al.*, 2013; *Sigmond et al.*, 2013].

217 We also assessed regional prediction skill for detrended SIE using a mean squared skill
218 score (MSSS) metric [*Murphy*, 1988; *Lindsay et al.*, 2008]. The regional skill differences in

MSSS are broadly consistent with the ACC results, showing highest skill in the North Atlantic sector and lower skill in the North Pacific and summer sea-ice regions (See Fig. S4).

3.2. Sources of Winter Regional Skill: Ocean Temperature Initialization

Next, we consider the physical mechanisms underlying the long-lead regional prediction skill for North Atlantic winter SIE. We first note that SIE anomalies in the Barents, Labrador, and GIN Seas are more persistent than anomalies in the Bering Sea and Sea of Okhotsk (See Fig. S3). This additional persistence contributes to the superior skill of North Atlantic SIE forecasts relative to their North Pacific counterparts. A key difference between the FLOR predictions and the persistence forecasts is that the FLOR predictions remain skillful over the summer initialization months, while persistence does not (compare Fig. 2 and Fig. S3 for the Barents, GIN, and Labrador Seas). These summer initialization months have little sea-ice coverage and, therefore, require another source of memory to provide winter SIE prediction skill. On these 4–11 month timescales, persistent anomalies in upper-ocean heat content represent a candidate source for this memory. Indeed, earlier work has shown that summer SST anomalies provide an important source of predictability for SIE anomalies in the ice-growth season [*Blanchard-Wrigglesworth et al.*, 2011b; *Day et al.*, 2014a; *Bushuk et al.*, 2014, 2015; *Bushuk and Giannakis*, 2015; *Sigmond et al.*, 2016; *Cheng et al.*, 2016; *Bushuk and Giannakis*, 2017]. In order to exploit the intrinsic memory of the ocean, the forecast system must be able to initialize and dynamically evolve ocean properties through the ice-free summer months and into the ice-growth season. To investigate this in the FLOR prediction system, we ask: Is there a relation between winter regional SIE and earlier ocean temperature ICs?

In Fig. 3 we plot correlation values, as a function of ocean depth and forecast lead time, between observed regional SIE and earlier regional-mean ocean temperature ICs. We focus on the Barents and Labrador Seas, due to the notably high skill in these regions. Before computing correlation values, both the SIE and ocean temperature time series are linearly detrended. The correlations are plotted for the upper 250m of the ocean, which is roughly the depth of the Barents Sea shelf region. The Labrador Sea is substantially deeper, but we focus on this upper-ocean region where the temperature correlations are strongest. We perform the analysis for regional-mean ocean temperatures because temperature anomalies are quite coherent over these regions (typical correlations between regional-mean values and spatial-gridpoint values are between 0.6 and 0.9). Using regional-mean temperatures allows us to move from four dimensions (latitude, longitude, depth, lead time) to two dimensions (depth and lead time), greatly simplifying the analysis.

Physically, one expects upper-ocean temperatures and regional SIE to negatively covary, since colder temperatures lead to more extensive sea ice, and vice versa. Indeed, we find clear negative correlations between observed winter Barents and Labrador SIE and the upper-ocean temperatures used to initialize the forecasts. This indicates that the data assimilation system is able to capture interannual fluctuations in surface and subsurface ocean temperatures in these regions. While the correlations are negative in both regions, their spatial structures are distinct. In the Labrador Sea, the strongest correlations are located within the mixed layer, and become surface intensified when the mixed layer shoals over the summer months. In contrast, the Barents Sea correlations are strongest beneath

the mixed layer for summer initialization months, and regain a surface signature for leads corresponding to initialization month May. This correlation structure closely resembles the mechanism for mid-latitude SST reemergence [*Alexander and Deser*, 1995; *Alexander et al.*, 1999], in which early-spring SST anomalies are stored beneath the summer mixed layer and reemerge to the surface when the mixed layer deepens the subsequent fall/winter. By this mechanism, summer subsurface ocean temperature anomalies have the potential to impact sea-ice growth rates the following fall/winter.

The correlation strengths in different target months reflect aspects of the SIE forecast skill shown in Fig. 2. In particular, the Barents Sea ocean correlations are weaker for target month March, consistent with the drop in skill in this month. Similarly, the Labrador Sea skill increases in March, consistent with the stronger temperature correlations at leads 8 and 9 in this month. Correlations between SIE and temperature ICs are generally lower in the Bering Sea and Sea of Okhotsk (See Fig. S5), which is consistent with the lower prediction skill in these regions.

The robust negative correlations in Fig. 3 indicate that the winter SIE forecast skill in the Barents and Labrador Seas is partially attributable to accurate initialization of upper-ocean temperatures. Due to imperfect observations and model biases, the ocean ICs produced by the assimilation system have errors relative to the true observed ocean state. Therefore, improving ocean initialization may be a promising route to improving winter SIE prediction skill. Indeed, the correlations between ocean temperature ICs and model-predicted SIE (See Fig. S6) are substantially higher than the correlations with observed SIE reported in Fig. 3. The difference between the model-predicted and observed

correlation values represents the potential skill improvements achievable via improved ocean initialization (See Fig. S7). The primary difference in these correlations is located beneath the summer mixed layer, suggesting a future need for improved subsurface ocean observations. Also, we find that the correlations with model-predicted SIE have less dependence on the mixed-layer depth than the correlations with observed SIE (compare Fig. S6 to Fig. 3). In particular, the Barents Sea correlations have larger values within and near the mixed layer, whereas the Labrador Sea displays larger values below the mixed layer. This suggests that the correlation structures in Fig. 3 do not necessarily reflect fundamental mechanisms of ice-ocean co-variability of this model, but instead may be partly associated with assimilation errors and/or model biases.

3.3. Sources of Summer Regional Skill: SIT Initialization

Next, we consider the sources of summer SIE prediction skill in the FLOR forecast system. Earlier work has shown that SIT is an important source of predictability for summer SIE on seasonal timescales [*Holland et al.*, 2011; *Blanchard-Wrigglesworth et al.*, 2011b; *Chevallier and Salas y Mélia*, 2012; *Lindsay et al.*, 2012; *Day et al.*, 2014b; *Germe et al.*, 2014; *Collow et al.*, 2015; *Guemas et al.*, 2016; *Bushuk et al.*, 2017]. The ECDA system does not directly assimilate SIT data, however it may implicitly capture interannual variations in SIT via its assimilation of atmospheric reanalysis data, which provides both thermodynamic and dynamic constraints on SIT. Lacking a long-term observational record of SIT, we compare ECDA SIT with the Pan-Arctic Ice Ocean Model and Assimilation System [PIOMAS; *Zhang and Rothrock*, 2003], which is an ice-ocean reanalysis that agrees quite well with available satellite and in situ SIT observations [*Schweiger et al.*,

2011]. ECDA is biased thin relative to PIOMAS by 0.5–1m, but captures similar interannual variability in sea-ice volume for all months of the year, with correlations ranging from 0.92–0.95 for total anomalies and 0.63–0.76 for detrended anomalies. Here, we examine the relationship between summer regional SIE and earlier SIT ICs, focusing on the East Siberian, Laptev, Beaufort, and Chukchi Seas.

In Fig. 4, we plot correlations between observed East Siberian Sea SIE and spatial-gridpoint values of SIT ICs in earlier months. Correlations are plotted for target months of June–September and lead times of 0–4 months. The linear trend is removed from both time series before the correlation is computed. We find that the local East Siberian SIE–SIT correlations are generally positive, consistent with the physical expectation that thicker initial sea ice should lead to more extensive summer sea ice, and vice versa. Moreover, we find that the SIE–SIT correlations have a diagonal structure that closely resembles the East Siberian ACC structure in Fig. 2. This diagonal structure implies that the SIT initialization month is crucially important in determining East Siberian SIE skill. In particular, the East Siberian SIE–SIT correlation values are similar for July lead-0, August lead-1, and September lead-2, which each correspond to July-initialized forecasts. Similarly, there is a correspondence between July lead-1, August lead-2, and September lead-3 (June initialization) and July lead-2, August lead-3, and September lead-4 (May initialization). These SIE–SIT correlations suggest that the summer SIE skill in the East Siberian Sea is partially attributable to accurate initialization of local SIT anomalies. Note that the SIE-SIT correlations using model-predicted SIE are slightly stronger, but also display a May prediction skill barrier (see Fig. S8). This suggests that the May bar-

rier is primarily related to the inherent predictability of East Siberian SIE, rather than resulting from SIT initialization errors.

SIT initialization also provides an important source of summer prediction skill in other Arctic regions with high summer SIE variability. Similar to the East Siberian Sea, we find that the SIE–SIT correlations in the Chukchi, Beaufort and Laptev Seas (See Figs. S9, S10, and S11, respectively) are consistent with the SIE prediction skill in these regions. The Chukchi Sea has SIE prediction skill up to leads of 4 months for target months June and July and lower skill for August and September (See Fig. 2). The Chukchi region displays strong SIE–SIT correlations for leads 0–4 in June and July, and correspondingly lower correlations in August and September (See Fig. S9). The Beaufort and Laptev Seas have similar prediction skill barriers to the East Siberian Sea (see the diagonal ACC structures in Fig. 2). The SIE–SIT correlations for these regions display a diagonal structure consistent with these skill barriers (see Figs. S10 and S11). These results demonstrate the importance of SIT ICs for summer SIE prediction and suggest that direct assimilation of thickness observations could potentially improve summer prediction skill.

4. Conclusions

This study has examined the seasonal prediction skill for Arctic regional SIE within the GFDL-FLOR dynamical forecast system. We have found that prediction skill for detrended regional SIE generally exceeds that of an anomaly persistence forecast. Prediction skill is notably high in the North Atlantic sector. Winter/spring Labrador SIE predictions are skillful at 7–11 month lead times, and predictions of winter SIE in the Barents and

GIN Seas are skillful at 5–9 month lead times. Forecast skill is lower in the North Pacific sector, partially due to the lower inherent persistence of regional SIE anomalies compared with their North Atlantic counterparts. Summer SIE forecasts are skillful at 1–4 month lead times in the East Siberian, Laptev, and Beaufort Seas, and exhibit prediction skill barriers in which skill drops off sharply in particular initialization months (May, May, and June, respectively).

We have found that the initial conditions of the GFDL-FLOR prediction system provide a crucial source of prediction skill for both winter and summer regional SIE. In particular, the high prediction skill for winter SIE in the Labrador and Barents Seas is partially attributable to the accurate initialization and persistence of surface and subsurface ocean temperature anomalies. Similarly, the summer SIE prediction skill in the East Siberian, Laptev, Beaufort, and Chukchi Seas is partially attributable to the accurate initialization and persistence of SIT anomalies.

This study has provided an overview of regional Arctic SIE prediction skill and highlighted some key physical mechanisms underlying this skill. These results demonstrate the key role of subsurface ocean and SIT observations in predictions of regional SIE, emphasizing the need to both maintain and improve existing Arctic observing systems. In addition to higher-quality observations, the route to improved regional predictions depends crucially on reducing model biases, optimizing coupled data assimilation techniques, and understanding the detailed physical mechanisms that impact regional SIE. The results of this study motivate future work in regional sea-ice prediction using this multi-faceted approach.

Acknowledgments. We thank Charlie Stock and Desiree Tomassi for stimulating discussions, and Dawei Li and Desiree Tomassi for comments on a preliminary version of this manuscript. This study was supported by NOAA's Climate Program Office, Climate Variability and Predictability Program (award GC15-504). The FLOR predictions analyzed in this work are available through the North American Multi-Model Ensemble (NMME) Phase-II data (http://www.cpc.ncep.noaa.gov/products/NMME/data.html). The NASA team sea-ice concentration observations used in this study are available from the National Snow and Ice Data Center website (http://nsidc.org/data/NSIDC-0051/versions/1).

References

Alexander, M. A., and C. Deser (1995), A mechanism for the recurrence of wintertime midlatitude SST anomalies, *J. Phys. Oceanogr.*, *25*(1), 122–137.

Alexander, M. A., C. Deser, and M. S. Timlin (1999), The reemergence of SST anomalies in the North Pacific Ocean, *J. Climate*, *12*, 2419–2433.

Bauer, P., A. Thorpe, and G. Brunet (2015), The quiet revolution of numerical weather prediction, *Nature*, *525*(7567), 47–55.

Bitz, C., M. Holland, A. Weaver, and M. Eby (2001), Simulating the ice-thickness distribution in a coupled climate model, *J. Geophys. Res.: Oceans*, *106*(C2), 2441–2463.

Blanchard-Wrigglesworth, E., C. Bitz, and M. Holland (2011a), Influence of initial conditions and climate forcing on predicting Arctic sea ice, *Geophys. Res. Lett.*, *38*(18).

Blanchard-Wrigglesworth, E., K. C. Armour, C. M. Bitz, and E. DeWeaver (2011b), Persistence and inherent predictability of Arctic sea ice in a GCM ensemble and observations, *J. Climate*, *24*, 231–250.

391 Blanchard-Wrigglesworth, E., R. Cullather, W. Wang, J. Zhang, and C. Bitz (2015),
392 Model forecast skill and sensitivity to initial conditions in the seasonal Sea Ice Outlook,
393 *Geophys. Res. Lett*, *42*(19), 8042–8048.
394 Bretherton, C. S., M. Widmann, V. P. Dymnikov, J. M. Wallace, and I. Bladé (1999),
395 The effective number of spatial degrees of freedom of a time-varying field, *J. Climate*,
396 *12*(7), 1990–2009.
397 Bushuk, M., and D. Giannakis (2015), Sea-ice reemergence in a model hierarchy, *Geophys.*
398 *Res. Lett.*, *42*, 5337–5345.
399 Bushuk, M., and D. Giannakis (2017), The seasonality and interannual variability of
400 Arctic sea-ice reemergence, *J. Climate*, doi:10.1175/JCLI-D-16-0549.1, in press.
401 Bushuk, M., D. Giannakis, and A. J. Majda (2014), Reemergence mechanisms for North
402 Pacific sea ice revealed through nonlinear Laplacian spectral analysis, *J. Climate*, *27*,
403 6265–6287.
404 Bushuk, M., D. Giannakis, and A. J. Majda (2015), Arctic sea-ice reemergence: The role
405 of large-scale oceanic and atmospheric variability, *J. Climate*, *28*, 5477–5509.
406 Bushuk, M., R. Msadek, M. Winton, G. Vecchi, R. Gudgel, A. Rosati, and X. Yang (2017),
407 Summer enhancement of Arctic sea-ice volume anomalies in the September-ice zone, *J.*
408 *Climate*, *30*, 2341–2362.
409 Cavalieri, D. J., and C. L. Parkinson (2012), Arctic sea ice variability and trends, 1979-
410 2010, *The Cryosphere*, *6*(4), 881–889, doi:10.5194/tc-6-881-2012.
411 Cavalieri, D. J., C. L. Parkinson, P. Gloersen, and H. J. Zwally (1996), Sea ice concentra-
412 tions from Nimbus-7 SMMR and DMSP SSM/I-SSMIS Passive Microwave Data, Version

413 1, *NASA DAAC at the Natl. Snow and Ice Data Cent.*, doi:10.5067/8GQ8LZQVL0VL.

414 Cheng, W., E. Blanchard-Wrigglesworth, C. M. Bitz, C. Ladd, and P. J. Stabeno (2016),
415 Diagnostic sea ice predictability in the pan-Arctic and US Arctic regional seas, *Geophys.*
416 *Res. Lett*, *43*(22).

417 Chevallier, M., and D. Salas y Mélia (2012), The role of sea ice thickness distribution in
418 the Arctic sea ice potential predictability: A diagnostic approach with a coupled GCM,
419 *J. Climate*, *25*(8), 3025–3038.

420 Chevallier, M., D. Salas y Mélia, A. Voldoire, M. Déqué, and G. Garric (2013), Seasonal
421 forecasts of the pan-Arctic sea ice extent using a GCM-based seasonal prediction system,
422 *J. Climate*, *26*(16), 6092–6104.

423 Collow, T. W., W. Wang, A. Kumar, and J. Zhang (2015), Improving Arctic sea ice
424 prediction using PIOMAS initial sea ice thickness in a coupled ocean–atmosphere model,
425 *Mon. Wea. Rev.*, *143*(11), 4618–4630.

426 Day, J., S. Tietsche, and E. Hawkins (2014a), Pan-Arctic and regional sea ice predictabil-
427 ity: Initialization month dependence, *J. Climate*, *27*(12), 4371–4390.

428 Day, J., E. Hawkins, and S. Tietsche (2014b), Will Arctic sea ice thickness initialization
429 improve seasonal forecast skill?, *Geophys. Res. Lett.*, *41*(21), 7566–7575.

430 Delworth, T. L., A. J. Broccoli, A. Rosati, R. J. Stouffer, V. Balaji, J. A. Beesley, W. F.
431 Cooke, K. W. Dixon, J. Dunne, K. Dunne, et al. (2006), Gfdl's CM2 global coupled
432 climate models. Part I: Formulation and simulation characteristics, *J. Climate*, *19*(5),
433 643–674.

Ford, J. D., and B. Smit (2004), A framework for assessing the vulnerability of communities in the Canadian Arctic to risks associated with climate change, *Arctic*, pp. 389–400.

Germe, A., M. Chevallier, D. S. y Mélia, E. Sanchez-Gomez, and C. Cassou (2014), Interannual predictability of Arctic sea ice in a global climate model: Regional contrasts and temporal evolution, *Climate Dynamics*, *43*(9-10), 2519–2538.

Guemas, V., M. Chevallier, M. Dqu, O. Bellprat, and F. Doblas-Reyes (2016), Impact of sea ice initialisation on sea ice and atmosphere prediction skill on seasonal timescales, *Geophys. Res. Lett*, *43*(8), 3889–3896.

Holland, M. M., D. A. Bailey, and S. Vavrus (2011), Inherent sea ice predictability in the rapidly changing Arctic environment of the Community Climate System Model, version 3, *Climate Dynamics*, *36*(7-8), 1239–1253.

Hunke, E., and J. Dukowicz (1997), An elastic-viscous-plastic model for sea ice dynamics, *J. Phys. Oceanogr.*, *27*(9), 1849–1867.

Jia, L., X. Yang, G. A. Vecchi, R. G. Gudgel, T. L. Delworth, A. Rosati, W. F. Stern, A. T. Wittenberg, L. Krishnamurthy, S. Zhang, et al. (2015), Improved seasonal prediction of temperature and precipitation over land in a high-resolution GFDL climate model, *J. Climate*, *28*(5), 2044–2062.

Jung, T., N. D. Gordon, P. Bauer, D. H. Bromwich, M. Chevallier, J. J. Day, J. Dawson, F. Doblas-Reyes, C. Fairall, H. F. Goessling, et al. (2016), Advancing polar prediction capabilities on daily to seasonal time scales, *Bull. Amer. Meteor. Soc.*, doi: 10.1175/BAMS-D-14-00246.1.

Koenigk, T., and U. Mikolajewicz (2009), Seasonal to interannual climate predictability in mid and high northern latitudes in a global coupled model, *Climate dynamics*, *32*(6), 783–798.

Krikken, F., M. Schmeits, W. Vlot, V. Guemas, and W. Hazeleger (2016), Skill improvement of dynamical seasonal Arctic sea ice forecasts, *Geophys. Res. Lett.*

Kwok, R., and D. Rothrock (2009), Decline in Arctic sea ice thickness from submarine and ICESat records: 1958–2008, *Geophys. Res. Lett.*, *36*(15).

Laliberté, F., S. Howell, and P. Kushner (2016), Regional variability of a projected sea ice-free Arctic during the summer months, *Geophys. Res. Lett.*, *43*(1), 256–263.

Levitus, S., J. Antonov, O. K. Baranova, T. Boyer, C. Coleman, H. Garcia, A. Grodsky, D. Johnson, R. Locarnini, A. V. Mishonov, et al. (2013), The world ocean database, *Data Science Journal*, *12*(0), WDS229–WDS234.

Lindsay, R., J. Zhang, A. Schweiger, and M. Steele (2008), Seasonal predictions of ice extent in the Arctic Ocean, *Journal of Geophysical Research: Oceans*, *113*(C2).

Lindsay, R., C. Haas, S. Hendricks, P. Hunkeler, N. Kurtz, J. Paden, B. Panzer, J. Sonntag, J. Yungel, and J. Zhang (2012), Seasonal forecasts of Arctic sea ice initialized with observations of ice thickness, *Geophys. Res. Lett*, *39*(21).

Maslanik, J., J. Stroeve, C. Fowler, and W. Emery (2011), Distribution and trends in Arctic sea ice age through spring 2011, *Geophys. Res. Lett*, *38*(13).

Melia, N., K. Haines, and E. Hawkins (2016), Sea ice decline and 21st century trans-Arctic shipping routes, *Geophys. Res. Lett.*, *43*, 97209728.

Merryfield, W., W.-S. Lee, W. Wang, M. Chen, and A. Kumar (2013), Multi-system seasonal predictions of Arctic sea ice, *Geophys. Res. Lett*, *40*(8), 1551–1556.

Msadek, R., G. Vecchi, M. Winton, and R. Gudgel (2014), Importance of initial conditions in seasonal predictions of Arctic sea ice extent, *Geophys. Res. Lett.*, *41*(14), 5208–5215.

Murphy, A. H. (1988), Skill scores based on the mean square error and their relationships to the correlation coefficient, *Monthly weather review*, *116*(12), 2417–2424.

Perovich, D. K., and C. Polashenski (2012), Albedo evolution of seasonal Arctic sea ice, *Geophys. Res. Lett*, *39*(8).

Peterson, K. A., A. Arribas, H. Hewitt, A. Keen, D. Lea, and A. McLaren (2015), Assessing the forecast skill of Arctic sea ice extent in the GloSea4 seasonal prediction system, *Climate Dynamics*, *44*(1-2), 147–162.

Petty, A. A., D. Schröder, J. Stroeve, T. Markus, J. Miller, N. Kurtz, D. Feltham, and D. Flocco (2017), Skillful spring forecasts of September Arctic sea ice extent using passive microwave sea ice observations, *Earth's Future*, *5*(2), 254–263.

Pizzolato, L., S. E. Howell, J. Dawson, F. Laliberté, and L. Copland (2016), The influence of declining sea ice on shipping activity in the Canadian Arctic, *Geophys. Res. Lett.*, *43*.

Regehr, E. V., N. J. Lunn, S. C. Amstrup, and I. Stirling (2007), Effects of earlier sea ice breakup on survival and population size of polar bears in western Hudson Bay, *The Journal of Wildlife Management*, *71*(8), 2673–2683.

Rigor, I. G., and J. M. Wallace (2004), Variations in the age of Arctic sea-ice and summer sea-ice extent, *Geophys. Res. Lett*, *31*(9).

Roemmich, D., S. Riser, R. Davis, and Y. Desaubies (2004), Autonomous profiling floats: Workhorse for broad-scale ocean observations, *Marine Technology Society Journal*, *38*(2), 21–29.

Rothrock, D. A., Y. Yu, and G. A. Maykut (1999), Thinning of the Arctic sea-ice cover, *Geophys. Res. Lett.*, *26*(23), 3469–3472.

Schröder, D., D. L. Feltham, D. Flocco, and M. Tsamados (2014), September Arctic sea-ice minimum predicted by spring melt-pond fraction, *Nature Climate Change*.

Schweiger, A., R. Lindsay, J. Zhang, M. Steele, H. Stern, and R. Kwok (2011), Uncertainty in modeled Arctic sea ice volume, *J. Geophys. Res.: Oceans*, *116*(C8).

Serreze, M. C., M. M. Holland, and J. Stroeve (2007), Perspectives on the Arctic's shrinking sea-ice cover, *Science*, *315*(5818), 1533–1536, doi:10.1126/science.1139426.

Sigmond, M., J. Fyfe, G. Flato, V. Kharin, and W. Merryfield (2013), Seasonal forecast skill of Arctic sea ice area in a dynamical forecast system, *Geophys. Res. Lett.*, *40*(3), 529–534.

Sigmond, M., M. Reader, G. Flato, W. Merryfield, and A. Tivy (2016), Skillful seasonal forecasts of Arctic sea ice retreat and advance dates in a dynamical forecast system, *Geophys. Res. Lett.*, *43*.

Smith, L. C., and S. R. Stephenson (2013), New Trans-Arctic shipping routes navigable by midcentury, *Proc. Natl. Acad. Sci.*, *110*(13), E1191–E1195.

Stock, C. A., K. Pegion, G. A. Vecchi, M. A. Alexander, D. Tommasi, N. A. Bond, P. S. Fratantoni, R. G. Gudgel, T. Kristiansen, T. D. OBrien, et al. (2015), Seasonal sea surface temperature anomaly prediction for coastal ecosystems, *Progress in Oceanography*,

137, 219–236.

Stroeve, J., T. Markus, L. Boisvert, J. Miller, and A. Barrett (2014a), Changes in Arctic melt season and implications for sea ice loss, *Geophys. Res. Lett*, *41*(4), 1216–1225.

Stroeve, J., L. C. Hamilton, C. M. Bitz, and E. Blanchard-Wrigglesworth (2014b), Predicting September sea ice: Ensemble skill of the SEARCH sea ice outlook 2008–2013, *Geophys. Res. Lett.*, *41*(7), 2411–2418.

Sun, C., A. Thresher, R. Keeley, N. Hall, M. Hamilton, P. Chinn, A. Tran, G. Goni, L. la VILLEON, T. Carval, et al. (2010), The data management system for the global temperature and salinity profile programme, *Proceedings of Ocean Obs*, *9*.

Tietsche, S., J. Day, V. Guemas, W. Hurlin, S. Keeley, D. Matei, R. Msadek, M. Collins, and E. Hawkins (2014), Seasonal to interannual Arctic sea ice predictability in current global climate models, *Geophys. Res. Lett.*, *41*(3), 1035–1043.

Van den Dool, H. (2006), *Empirical Methods in Short-Term Climate Prediction*, Oxford Univ. Press, Oxford, U. K.

Vecchi, G. A., T. Delworth, R. Gudgel, S. Kapnick, A. Rosati, A. T. Wittenberg, F. Zeng, W. Anderson, V. Balaji, K. Dixon, et al. (2014), On the seasonal forecasting of regional tropical cyclone activity, *J. Climate*, *27*(21), 7994–8016.

Wang, L., X. Yuan, M. Ting, and C. Li (2016), Predicting summer Arctic sea ice concentration intraseasonal variability using a vector autoregressive model*, *J. Climate*, *29*(4), 1529–1543.

Wang, W., M. Chen, and A. Kumar (2013), Seasonal prediction of Arctic sea ice extent from a coupled dynamical forecast system, *Mon. Wea. Rev.*, *141*(4), 1375–1394.

Winton, M. (2000), A reformulated three-layer sea ice model, *J. Atmos. Oceanic Technol.*, *17*(4), 525–531.

Wyllie-Echeverria, T., and W. S. Wooster (1998), Year-to-year variations in Bering Sea ice cover and some consequences for fish distributions, *Fisheries Oceanography*, *7*(2), 159–170.

Yeager, S. G., A. R. Karspeck, and G. Danabasoglu (2015), Predicted slowdown in the rate of Atlantic sea ice loss, *Geophysical Research Letters*, *42*(24).

Yuan, X., D. Chen, C. Li, L. Wang, and W. Wang (2016), Arctic sea ice seasonal prediction by a linear markov model, *J. Climate*, *29*(22), 8151–8173.

Zhang, J., and D. Rothrock (2003), Modeling global sea ice with a thickness and enthalpy distribution model in generalized curvilinear coordinates, *Mon. Wea. Rev.*, *131*(5), 845–861.

Zhang, S., M. Harrison, A. Rosati, and A. Wittenberg (2007), System design and evaluation of coupled ensemble data assimilation for global oceanic climate studies, *Mon. Wea. Rev.*, *135*(10), 3541–3564.

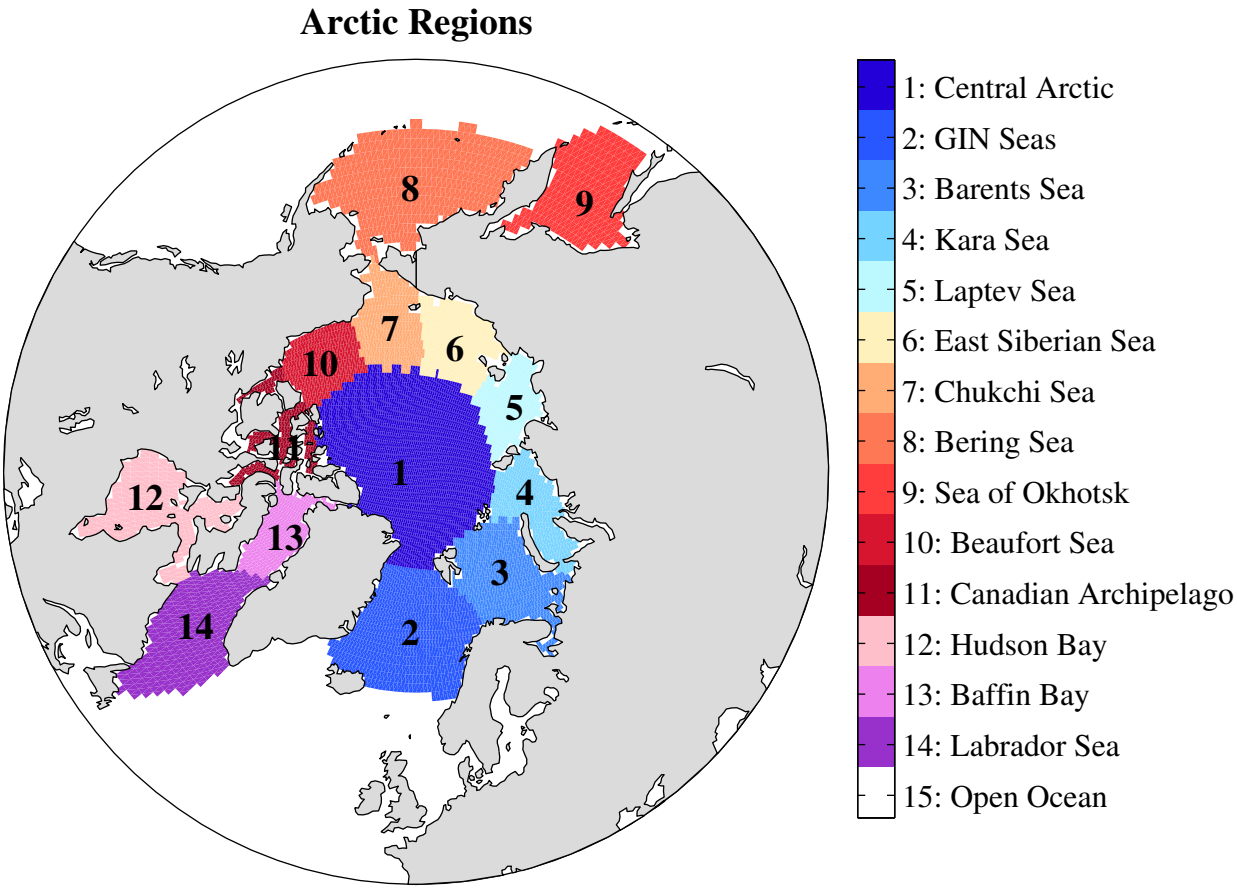

Figure 1. The Arctic regions considered in this study.

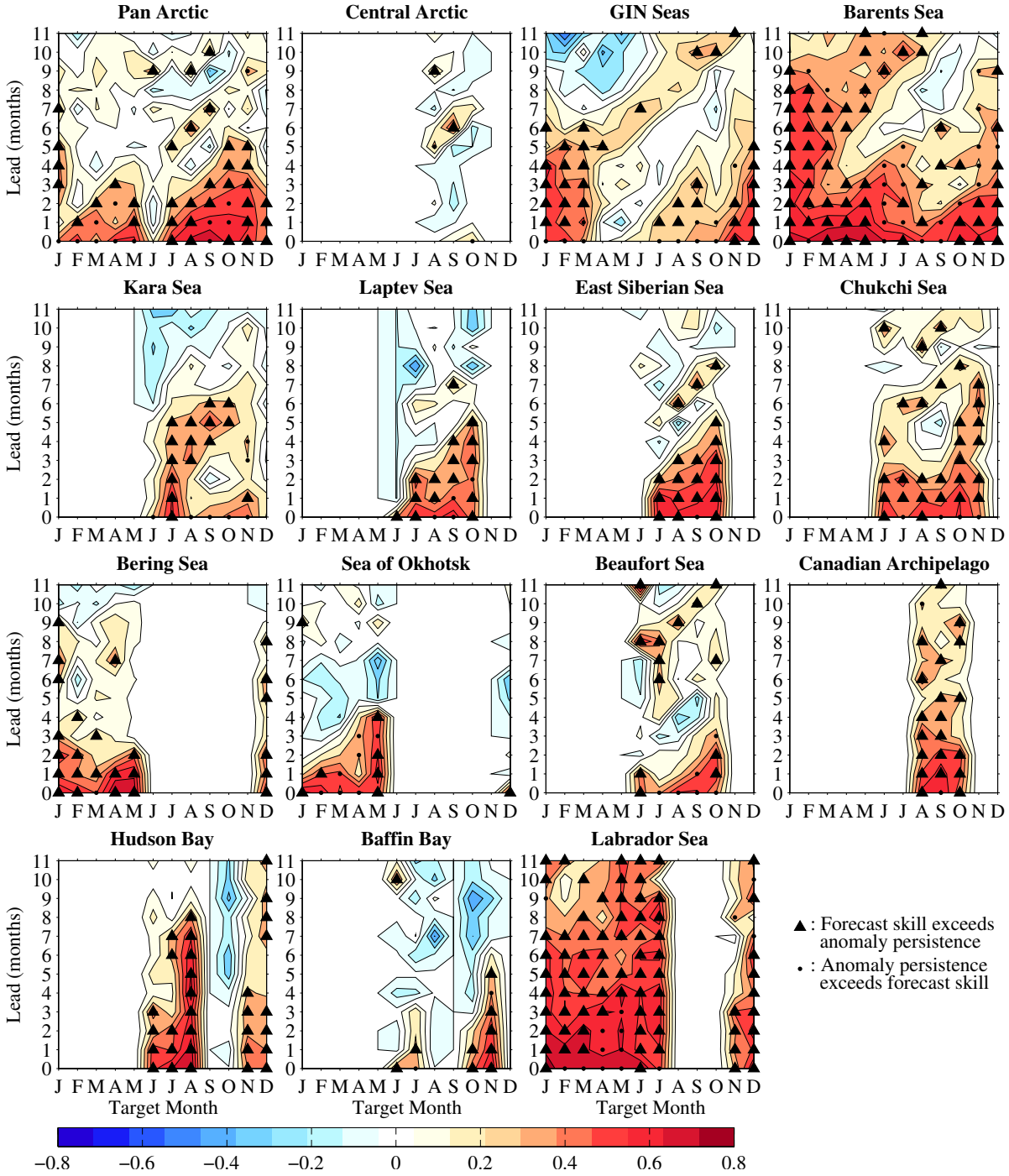

Figure 2. Seasonal prediction skill (ACC) for detrended regional Arctic SIE. The triangle and dot markers indicate months in which the ACC values are statistically significant at the 95% confidence level. Triangles indicate months in which the dynamical model's skill exceeds that of a persistence forecast and circles indicate months in which the persistence forecast exceeds the model's skill. Correlations are only plotted for target months with SIE standard deviation greater than 0.03 million km^2.

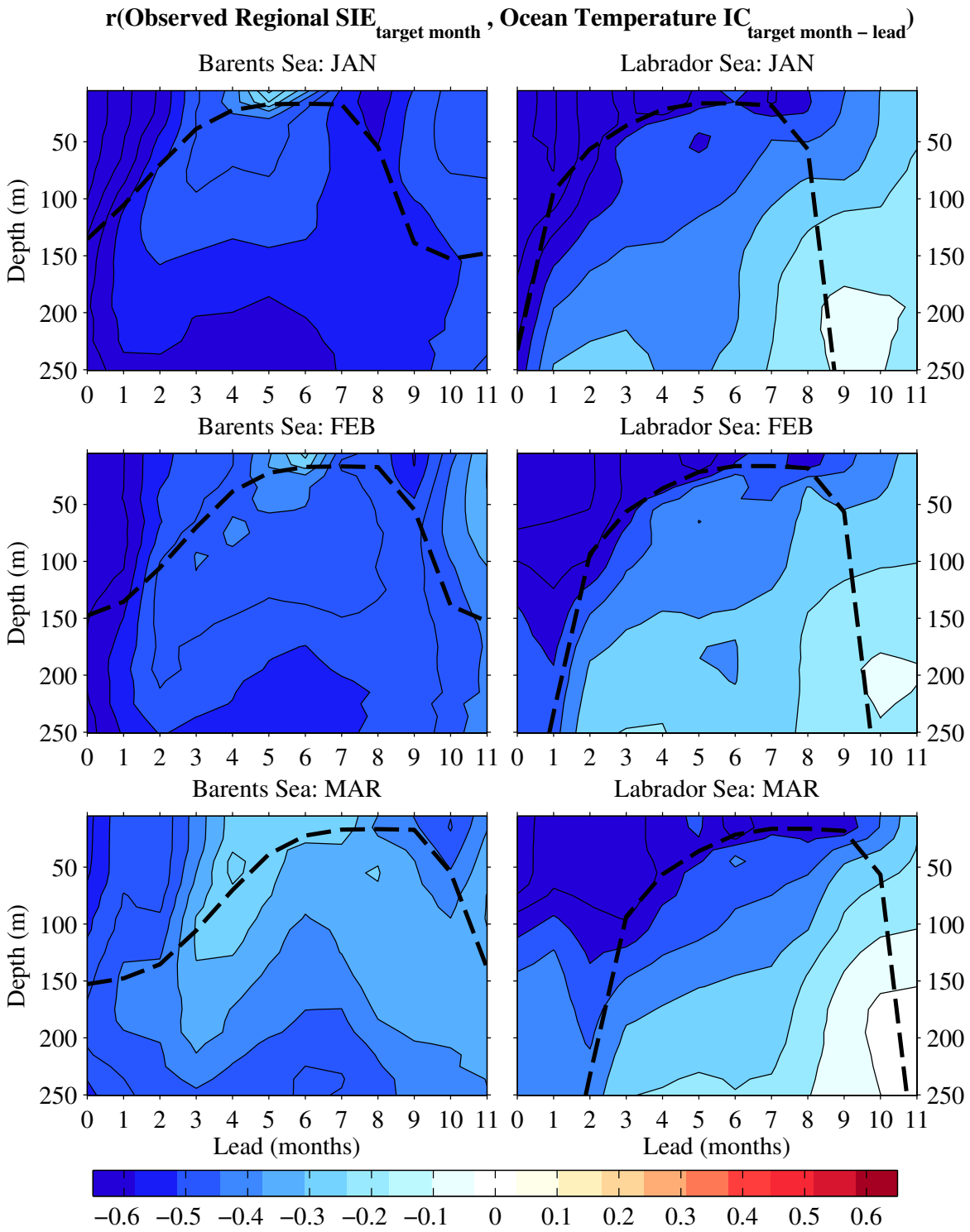

Figure 3. Correlation between observed regional SIE and regional-mean ocean temperature ICs in earlier months. Correlations are plotted as a function of ocean depth and forecast lead time for the Barents and Labrador Seas and target months of January–March. The linear trend is removed from both time series before the correlation is computed. The regional-mean mixed-layer depth climatology is plotted as dashed lines. Correlation values satisfying $|r| > 0.34$ are statistically significant at the 95% level.

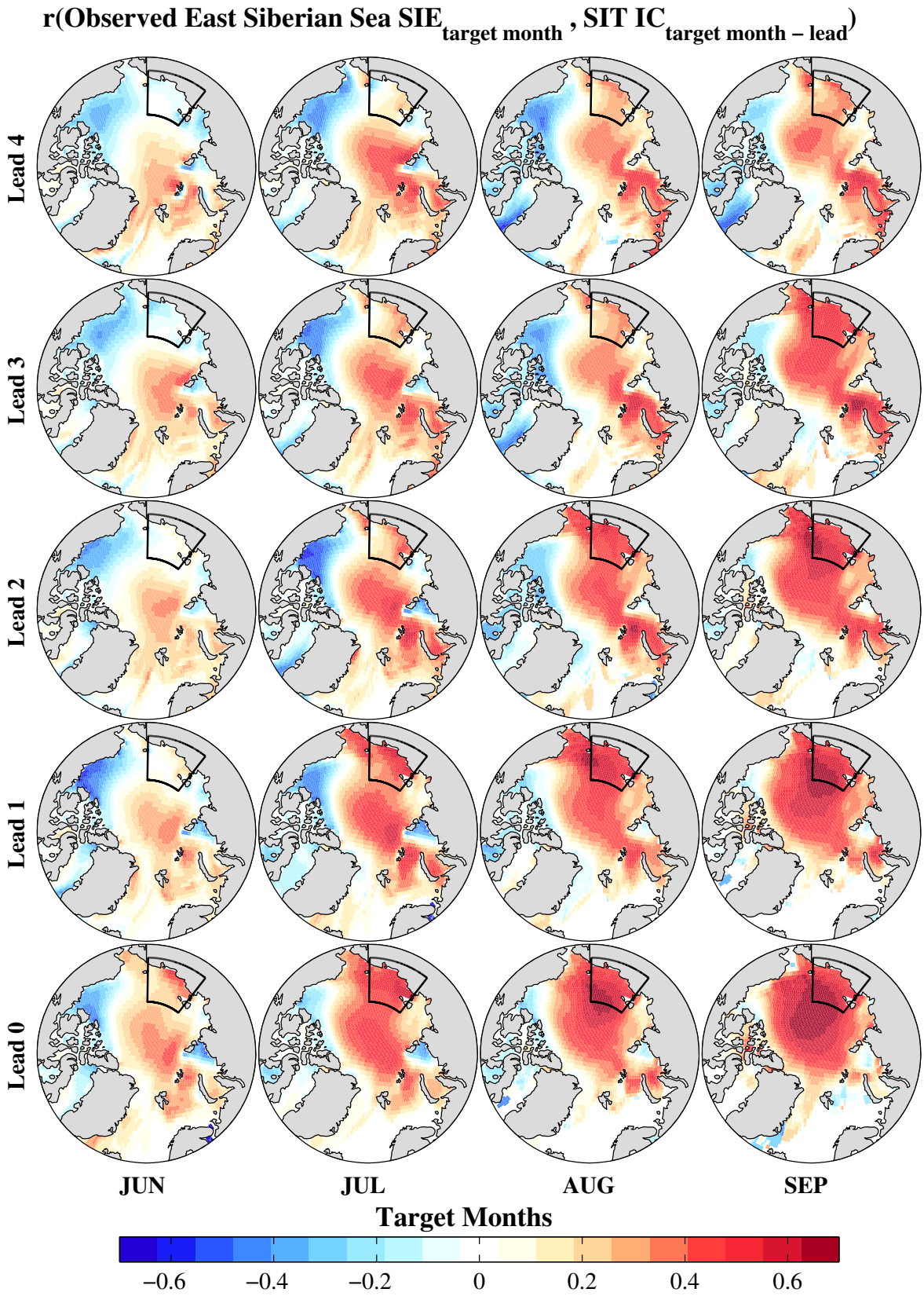

Figure 4. Correlations between observed East Siberian (boxed area) SIE and SIT ICs for different target months and forecast lead times. The linear trend is removed from both time series before the correlation is computed.